Hydrothermal Synthesis of CuO-SnO$_2$ and CuO-SnO$_2$-Fe$_2$O$_3$ Mixed Oxides and their Electrochemical Characterization in Neutral Electrolyte

M. Jayalakshmi[*], *K. Balasubramanian*

Non-Ferrous Materials Technology Development Centre (NFTDC), Kanchanbagh Post, Hyderabad- 500058, India.
[*]E-mail: jayalakshmi@nftdc.res.in

Hydrothermal synthesis of CuO-SnO$_2$ and CuO-SnO$_2$-Fe$_2$O$_3$ mixed oxides is done in an autoclave using the precursors and urea. The powders are characterized by XRD, XRF, SEM and XPS. Their electrochemical behavior is studied using cyclic voltammgorams in 0.1 M KCl solution. Introduction of Fe$_2$O$_3$ to CuO-SnO$_2$ increased the capacitances by twofold which decreased on continuous cycling, approaching a limiting value. The changes in electrochemical capacitances are explained based on the hypothetical band alignment of p-type CuO, Fe$_2$O$_3$ and n-type SnO$_2$. The decrease in electrochemical capacitances on cycling has been attributed to the passive film formation on the surface of the mixed oxide electrode surfaces.

1. INTRODUCTION

New materials that can be used as electrodes in electrochemical double layer capacitors (EDLC) or super capacitors are synthesized and studied intensively in recent times in view of their importance in hybrid electric vehicle, memory back up devices and innumerable varieties of electronic appliances. We published very recently an over view on the electrode materials that have been tried for application in EDLCs/super capacitors [1]. Mixed metal oxides are preferred to single oxides as one or more oxides help in augmenting the capacitances as they tend to be complementary in their properties. Some examples are: Pb$_2$Ru$_2$O$_{6.5}$ [2], cobalt-nickel oxide/CNT composite [3], Ti/RhO$_x$ + Co$_3$O$_4$ [4],

NiO/RuO$_2$ [5], Ru$_{1-y}$Cr$_y$O$_2$ loaded on TiO$_2$ nanotubes [6], SnO$_2$- Al$_2$O$_3$, SnO$_2$- Al$_2$O$_3$-Carbon [7], SnO$_2$-V$_2$O$_5$, SnO$_2$-V$_2$O$_5$-CNT [8], SnO$_2$–Fe$_3$O$_4$, SnO$_2$–RuO$_2$ [9] and Ir$_{0.3}$Mn$_{0.7}$O$_2$ [10,11]. Considering the typical example of V$_2$O$_5$, it is known that it has modest electronic properties. In combination with SnO$_2$, it's electronic and redox properties gets improvised so that higher electrochemical capacitances are achieved [8]. In catalytic applications, it is known that SnO$_2$ is different from other more conventional supports; it exhibits efficient semi-conductivity together with conventional redox properties. In combination with V$_2$O$_5$, SnO2 forms a catalyst that is capable of promoting many organic conversions. In effect, SnO$_2$ enhances the use ratio of V$_2$O$_5$ to a different dimension [12].

We report in the present work, hydrothermal synthesis of CuO-SnO$_2$ and CuO-SnO$_2$-Fe$_2$O$_3$ mixed oxides using urea as the hydrolytic agent and their electrochemical behavior by cyclic voltammetry (CV). The powders were characterized by X-ray diffraction (XRD), X-ray fluorescence (XRF), Scanning electron microscopy (SEM) and X-ray photoelectron spectroscopy (XPS). An attempt to understand the capacitance output of mixed oxides by band edge alignment is also done.

2. EXPERIMENTAL PART

2.1. Hydrothermal Synthesis of mixed oxides

2.1.1. CuO -SnO$_2$

Cu(NO$_3$)$_2$.3H$_2$O (0.05 mol) and SnCl$_2$.2H$_2$O (0.05 mol) were initially dissolved in 250 ml of water and then urea (0.2 mol) was added to the homogeneous mixture and transferred to an autoclave. The solution was allowed to reach to 180 °C within an hour (ramp time). The reaction was kept at this temperature for 2 hours (soak time) with an in-situ pressure of 12 atmospheres. After 2 hours, it was cooled to room temperature. The product was filtered, washed with water and acetone and dried at 110 °C in a hot air oven. The initial pH of the experimental solution was acidic (pH ~ 4) and the final pH was alkaline (pH ~8). The final product was pale green in color.

2.1.2. CuO-SnO$_2$-Fe$_2$O$_3$

Cu(NO$_3$)$_2$.3H$_2$O (0.05 mol), FeCl$_2$.4H$_2$O (0.05 mol) and SnCl$_2$.2H$_2$O (0.05 mol) were initially dissolved in 250 ml of water and then urea (0.2 mol) was added to the homogeneous mixture and transferred to an autoclave. The solution was allowed to reach to 180 °C within an hour (ramp time). The reaction was kept at this temperature for 2 hours (soak time) with an in-situ pressure of 12 atmospheres. After 2 hours, it was cooled to room temperature. The product was filtered, washed with water and acetone and dried at 110 °C in a hot air oven. The initial pH of the experimental solution was acidic (pH ~ 4) and the final pH was alkaline (pH ~8). The final powder was reddish brown in color.

2.2. Instrumentation

All electrochemical experiments were conducted with a PGSTAT 30 Autolab system (Ecochemie, Utrecht, The Netherlands). It was connected to a PC running with Eco-Chemie GPES software. GPES software was used for all electrochemical data analysis. The reference electrode was Ag/AgCl (3M KCl) and the counter electrode was a platinum foil supplied along with the instrument. The electrolyte solution was 0.1 M KCl. Paraffin impregnated graphite electrodes (PIGE) were used as working electrodes with the surface immobilized with the active electrode materials. A few micrograms of mixed oxide nano-particles were placed on a clean glass plate and the surface of PIGE electrode was pressed over the nano-material which would mechanically transfer the nano-particles to the tip of the electrode. This method is highly successful to study the electrochemical properties of new inorganic materials without disturbing the grain size or surface area [13].

Powder XRD data of the samples were obtained by means of a Siemens D 5000 X-ray diffractometer with Bragg–Brentano geometry and having Cu Kα radiation ($\lambda = 1.5418$ °A). SEM-EDAX analysis was done using scanning electron microscope, Leo 440 (Germany). X-ray fluorescence measurements were carried out in a PW 2400 Philips make.

3. RESULTS AND DISCUSSION

3.1. Materials Characterization

X-ray fluorescence measurements of $CuO-SnO_2$ showed 96.47 % SnO_2 and 3.53% CuO and that of $CuO-SnO_2-Fe_2O_3$ to be 57.86% SnO_2, 4.87% CuO and 37.26% Fe_2O_3. XPS analysis of $CuO-SnO_2$ showed copper ions in the cupric state (figure not given). Fig. 1 shows the XRD pattern and SEM image of $CuO-SnO_2$; the diffraction peaks can be indexed to SnO_2 as per the JCPDS file 88-0287. The dominance of SnO_2 over copper oxide in their mixed oxide was reported earlier. The researchers claimed that the CuO has entered the crystal lattice and SnO_2-CuO solid solution is formed but at relatively high temperatures [14]. In our earlier works, on mixed oxides, we observed similar behavior for $SnO_2-Al_2O_3$ and $SnO_2 -V_2O_5$ mixed oxides synthesized by hydrothermal method; the temperature of the autoclave was 180°C [7, 8]. The XRD pattern of $SnO_2-Al_2O_3$ did not show the diffraction peaks due to Al_2O_3 but its presence in the mixed oxide was proved by EDAX and ICP-AES elemental analysis. Likewise, the XRD pattern of $SnO_2 -V_2O_5$ mixed oxide did not show the diffraction peaks due to V_2O_5 but its presence was proved by Raman spectra. Fig. 2 shows the XRD pattern and SEM image of $CuO-SnO_2-Fe_2O_3$ mixed oxide; the diffraction peaks can be indexed to Fe_2O_3 as per the JCPDS file 89-0599 though the presence of CuO and SnO_2 was confirmed by XRF data. The reason for this anomalous behavior is not clear and requires detailed investigation which is beyond the scope of the present work.

The morphology of $CuO-SnO_2$ mixed oxide reflects larger platelets of SnO_2 dispersed with much smaller CuO particles (Fig. 1). Particle sizes range from 47 to 500 nm. The morphology of CuO-

SnO_2-Fe_2O_3 differed entirely from the binary oxide. The particles were almost spherical in shape and their sizes were in the range of 30 to 76 nm (Fig. 2).
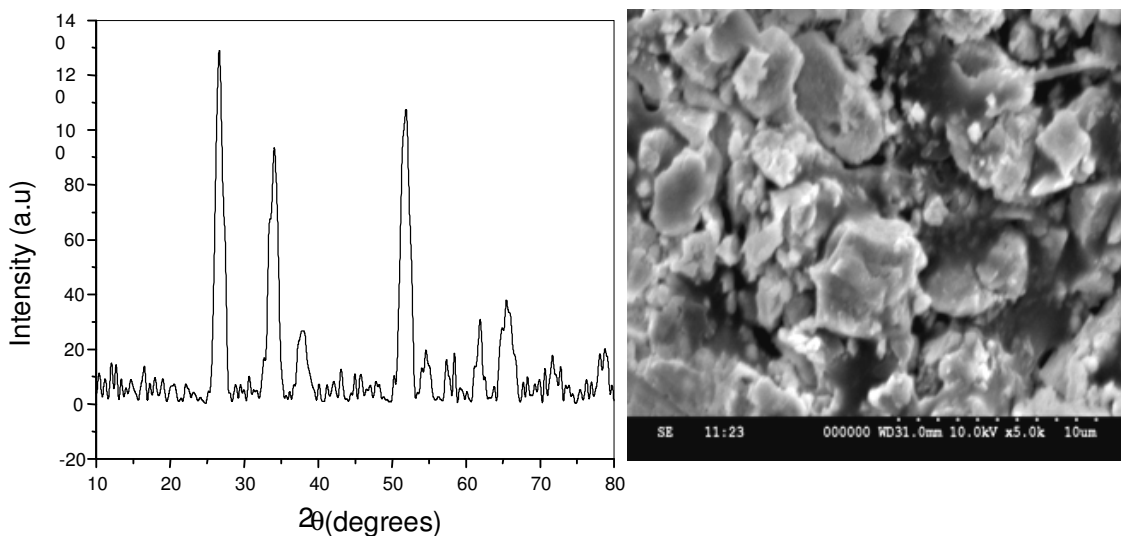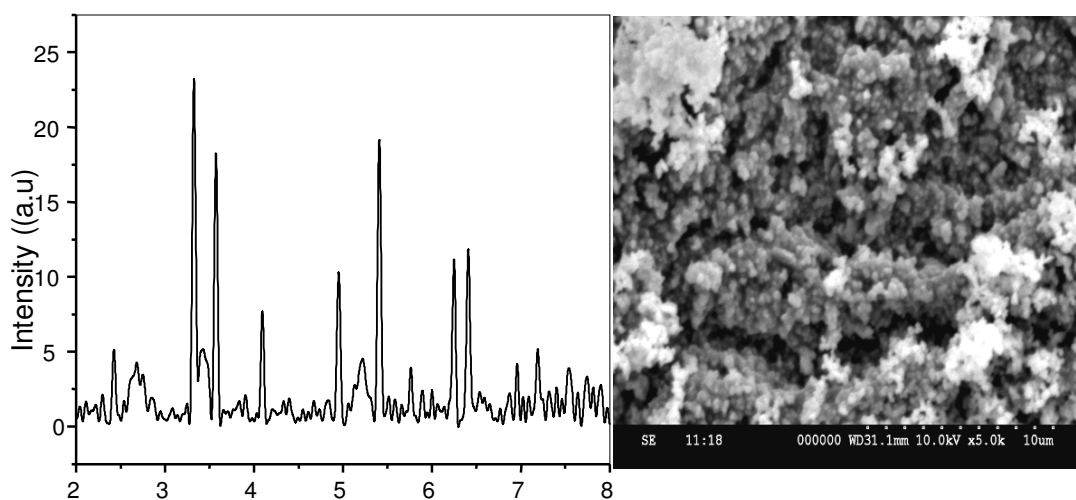

Figure 1. XRD pattern and SEM image of CuO-SnO_2 powder

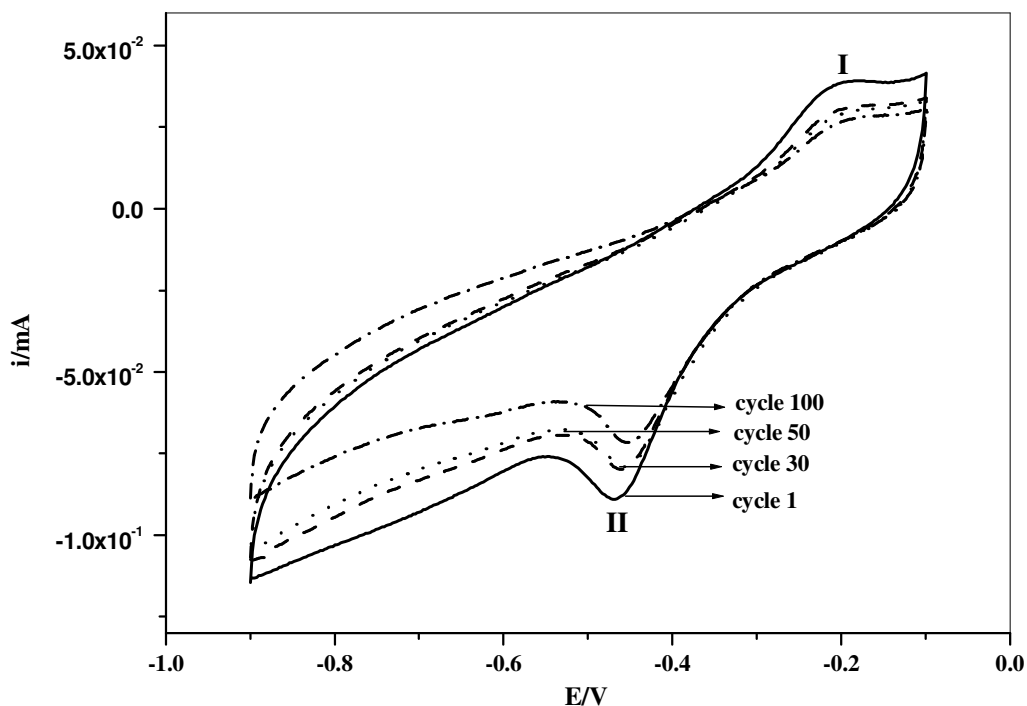**Figure 2**. XRD pattern and SEM image of CuO-SnO_2-Fe_2O_3 powder

Figure 3. Cyclic voltammograms of CuO powder immobilized on PIGE and recorded in 0.1 M KCl solution at 1st, 30th, 50th and 100th cycles; Scan rate = 50 mVs^{-1}.
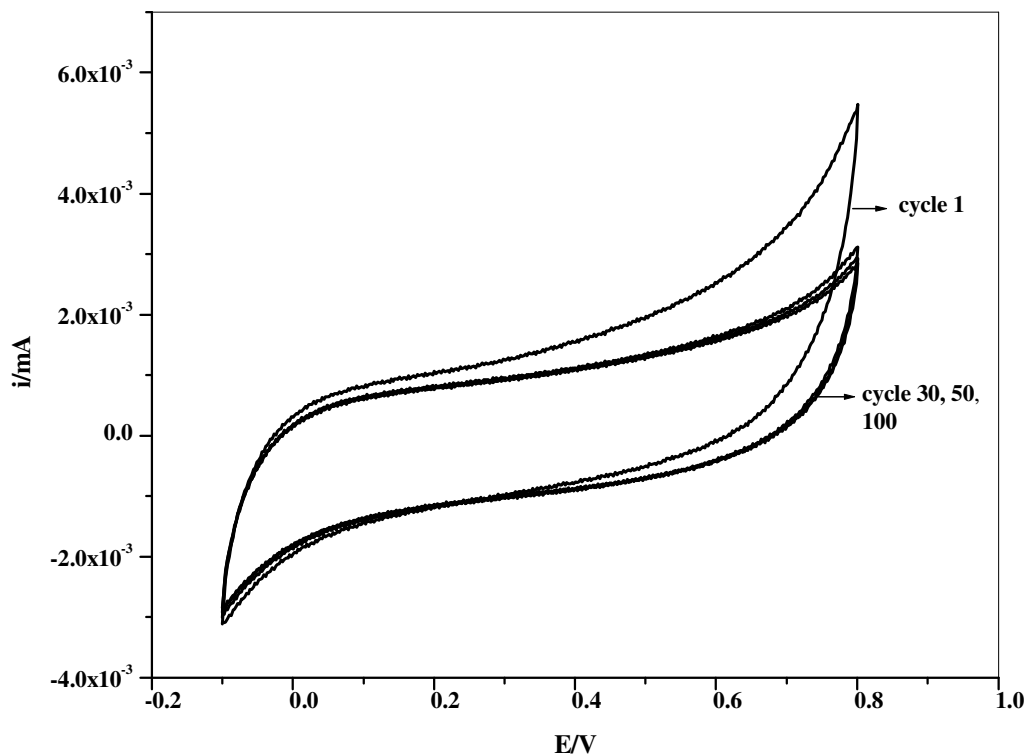

Figure 4. Cyclic voltammograms of CuO-SnO$_2$ powder immobilized on PIGE and recorded in 0.1 M KCl solution at 1st, 30th, 50th and 100th cycles; Scan rate = 50 mVs^{-1}.

3.2. Cyclic voltammetric studies

Fig. 3 shows the cyclic voltammograms (CVs) recorded for CuO (commercial grade) in 0.1 M KCl electrolyte. The potential window of the CVs is from -0.9 to -0.1 V vs. Ag/AgCl. It is well known that CuO produces only redox peaks pertaining to the cupric state in neutral salt solutions. In our earlier work, the CVs recorded for SnO_2 in 0.1 M KCl solution showed the typical I-V response of electrochemical capacitor within the potential limits of -0.3 to 1.25 V vs. Ag/AgCl [15]. Fig. 4 presents the CVs recorded for CuO-SnO_2 in 0.1 M KCl electrolyte for various scans at the scan rate of 50 mVs^{-1}. The CVs characteristics resemble more of SnO_2 rather than CuO in terms of shape and potential window (0.1 to 0.8 V). Table 1 presents the electrochemical capacitances calculated for SnO_2, CuO and CuO-SnO_2 at the scan rate of 50 mVs^{-1}. It could be seen that the values are comparatively less for the mixed oxide as against the single oxides.

Table 1. Electrochemical capacitances calculated for the oxides from the cyclic voltammograms for the recorded first and 100th scan; $\upsilon = 50$ mV/s

Electrode	Electrochemical capacitance (F/g)	
	Scan 1	Scan 100
CuO	32.0	24.0
SnO_2*	17.4	17.5
CuO-SnO_2	3.20	1.98
CuO-SnO_2-Fe_2O_3	7.33	3.13

* Capacitance values for SnO_2 are taken from ref. 15

The CuO-SnO_2 electrode's performance may be understood by borrowing some basic ideas from semiconductor physics. In our earlier work on ZnS, large voltage obtained in neutral solutions is ascribed to band edge bendings (conduction band and valence band) associated with positive and negative ion adsorption at the interface of semiconductor ZnS/solution [16]. Similarly, in suphur, carbon and nitrogen doped TiO_2 nanoparticles, the cyclic voltammetric response of doped titania showed an induced charge transfer giving rise to anodic and cathodic peaks; this interesting and significant observation was understood in termd of band bending due to anion doping as well as to the pH changes in experimental solutions [17]. It is known that Fermi level (or strictly speaking, chemical potential) of any two solids in contact must be in thermal equilibrium. Both may have different work functions (i.e the difference between the Fermi energy and the vacuum level) and if so, when the two materials are placed in contact, electrons will flow from the one with the lower work function until the Fermi levels equilibrate. CuO is a p-type semiconductor with a band gap of 1.35 eV and SnO_2 is an n-type semiconductor with a band gap of 3.8 eV. If the electrons flow from SnO_2 to CuO, then the resulting electrostatic potential leads to a built-in-filed; this built-in-field is responsible for the band

bending in the semiconductor near junction. Once the mixed oxide is exposed to aqueous solution, the Fermi level gets pinned due to charges that accumulate at the oxide/solution interface which is entirely an electrochemical phenomenon. The reason for the appearance of CVs in Fig. 4 (for CuO-SnO$_2$) resembling the CV characteristics of SnO$_2$ rather than CuO may thus be understandable.

In the mixed oxide however, the reasons for the decrease in electrochemical capacitance as compared to the single oxide need to be examined. While oxygen-deficient SnO$_2$ shows n-type conductivity by electrons, oxygen-excess CuO shows p-type conductivity by holes. At the grain boundaries, n-p-n heterojunctions lead to space charge and the magnitude of this space charge depends on the amount of CuO present in the mixed oxide. The resistance of the sample arises from two factors: n-p-n heterojunctions formed at the grain boundaries and barriers between SnO$_2$ grains due to oxygen absorption on the surface [18, 19]. As long as the p-n heterojunctions exist in the mixed oxide, this ohmic resistance remains intact. This inherent resistance of the sample reduces the homogenous accumulation of electrons at the double layer, decreasing the net charge separation so that the electrochemical capacitance of the mixed oxide decreases as compared to either single oxide. Fig. 5 shows the band structure for CuO-SnO$_2$. There exists a potential barrier between Ec (conduction band) of CuO and that of SnO$_2$ in the solid state but the equilibration of Fermi level followed by pinning on exposure to alkali solution may alleviate this potential barrier so that electrons tunnel through the transitional layer, leading to the electrochemical response as shown in Fig. 4 and a band structure as shown in Fig. 5.
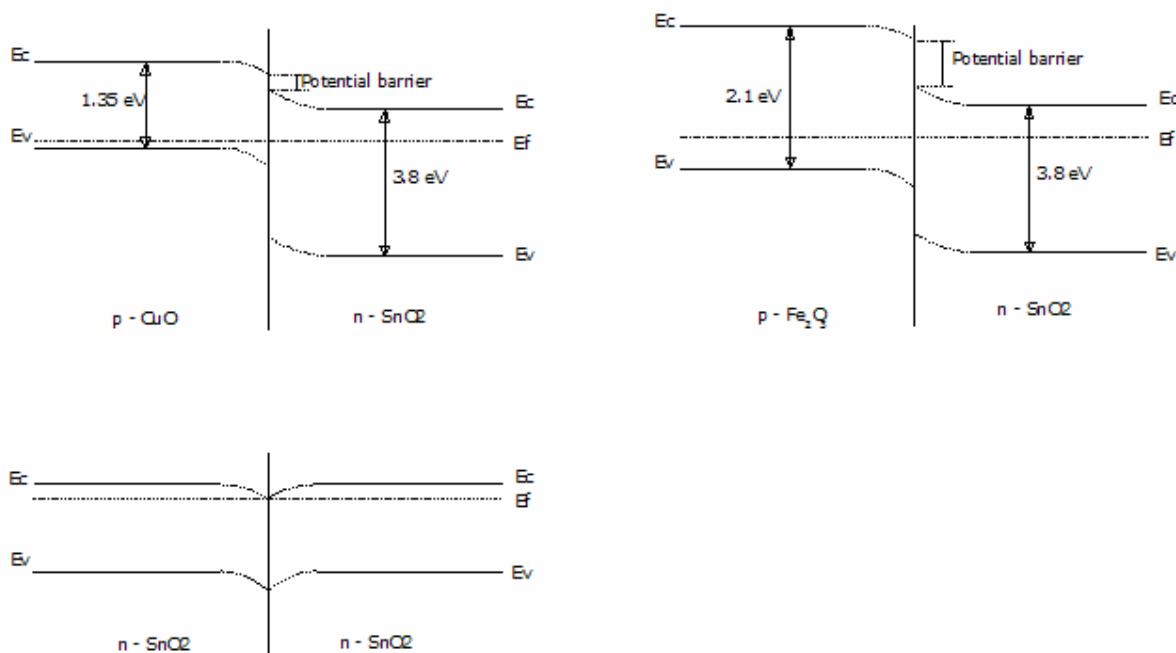

Figure 5. Hypothetical band alignment of CuO and SnO$_2$ in contact with each other and band bending in presence of aqueous solution
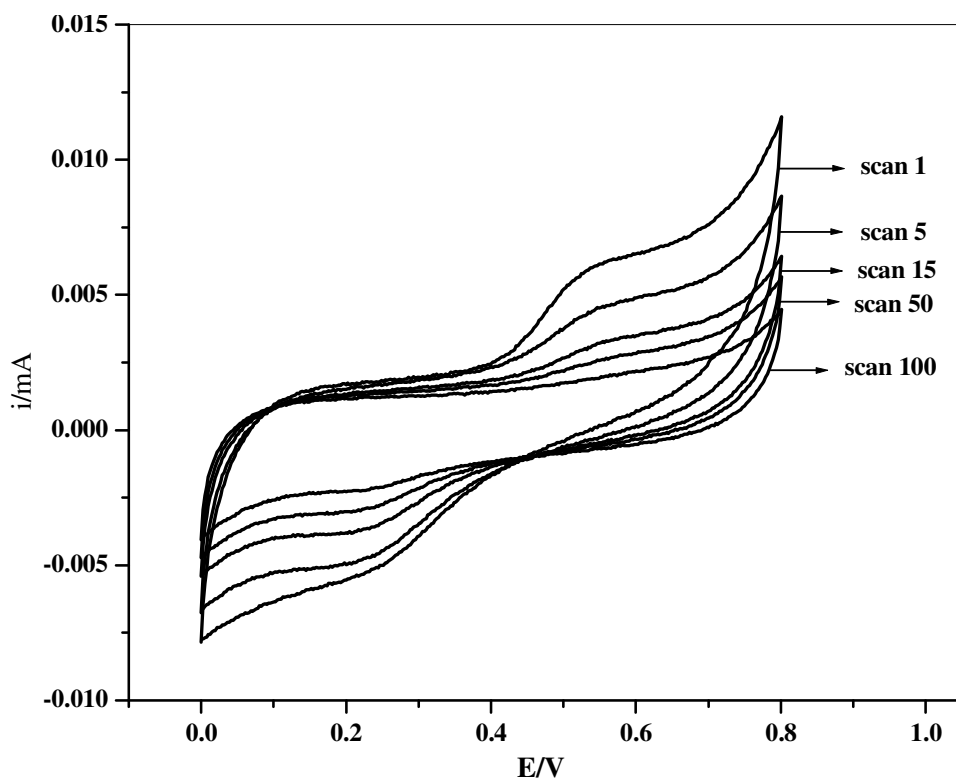
Figure 6. Cyclic voltammograms of CuO-SnO$_2$-Fe$_2$O$_3$ powder immobilized on PIGE and recorded in 0.1 M KCl solution at 1st, 5th, 15th, 50th and 100th cycles; Scan rate = 50 mVs^{-1}.
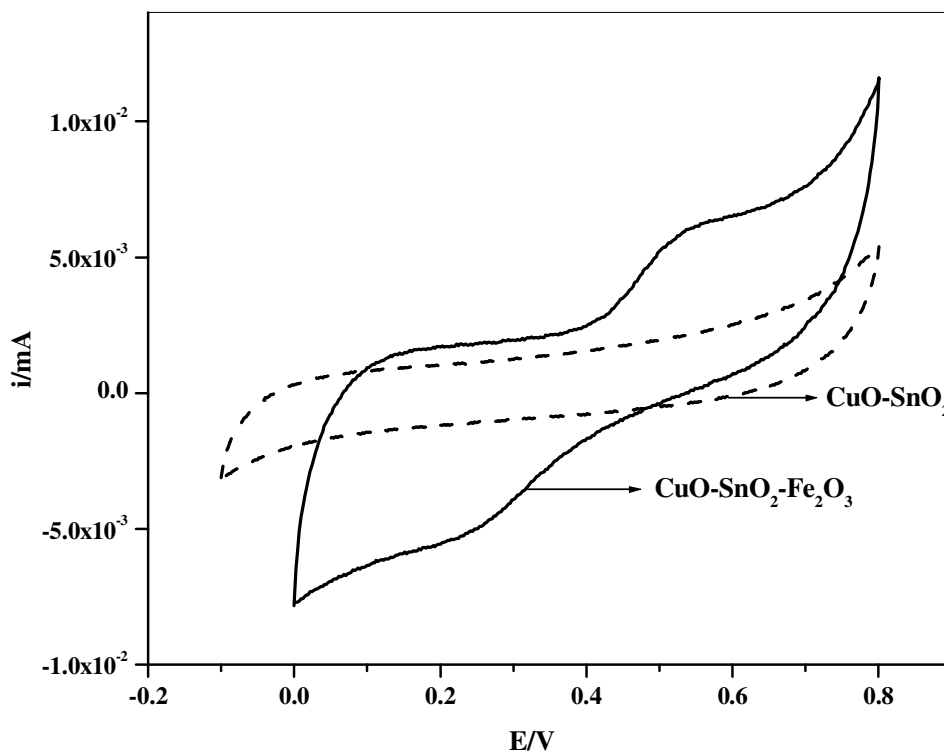

Figure 7. Cyclic voltammograms of CuO-SnO$_2$ and CuO-SnO$_2$-Fe$_2$O$_3$ powders in 0.1 M KCl solution at the initial scan; Scan rate = 50 mVs^{-1}.
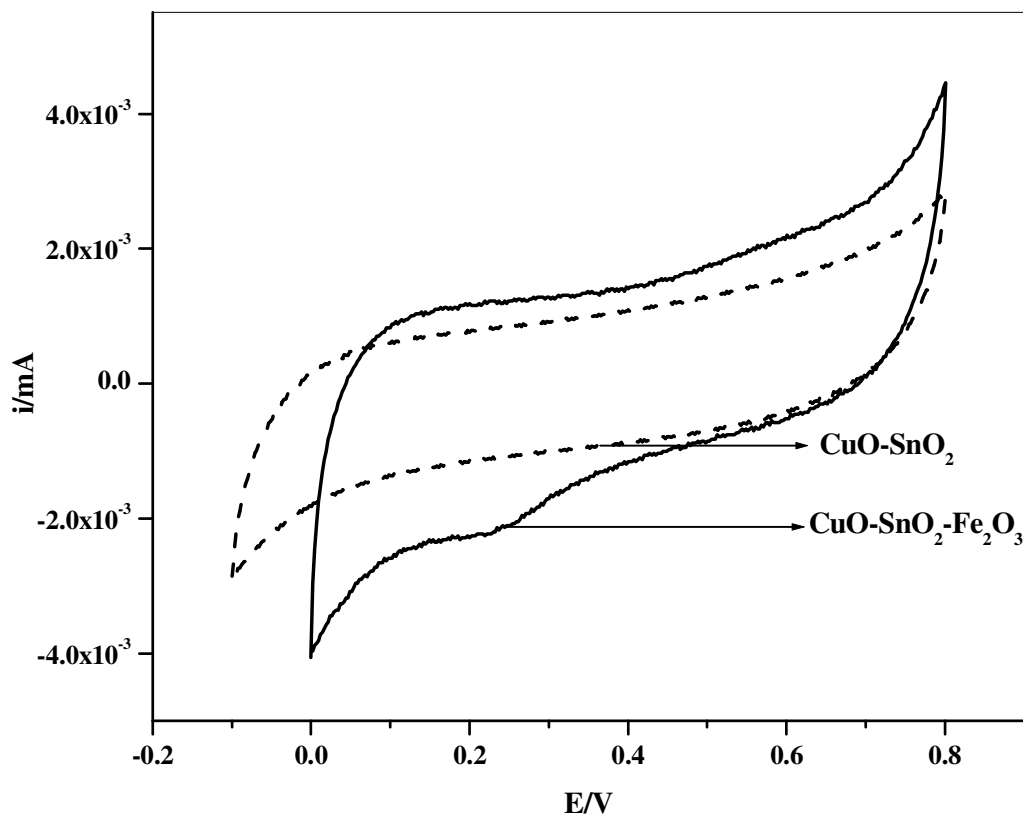
Figure 8. Cyclic voltammograms of CuO-SnO_2 and CuO-SnO_2-Fe_2O_3 powders in 0.1 M KCl solution at the 100th scan; Scan rate = 50 mVs^{-1}.

The basic interest in studying the electrochemical behavior of this ternary oxide, CuO-SnO_2-Fe_2O_3 lies in the fact whether the addition of Fe_2O_3 to CuO-SnO_2 (a n-type semiconducting oxide with a band gap of 2.1 eV) improves the electrochemical capacitance of the system. The results are interesting; the presence of Fe_2O_3 did increase the performance in the initial stages of cyclic polarization but started decreased on continuous cycling to 100 scans. Fig. 6 shows the CVs of CuO-SnO_2-Fe_2O_3 for the various scans recorded at the scan rate of 50 mVs^{-1}. The initial scans show a quasi reversible set of redox peaks (anodic peak, 0.55 V; cathodic peak, 0.2 V) appearing due to Fe (II) $\leftrightarrow$ Fe (III) transition; this faradic reaction contributed to a two-fold increase in electrochemical capacitance as compared to the binary oxide. However, on continuous cycling, the CV behavior changes gradually to that of a typical electrochemical capacitor but with considerable decrease in net capacitance (i.e faradic + non-faradic capacitance). This change is well illustrated in Fig. 7 and 8 which demonstrate the difference in electrochemical behavior of both binary and ternary mixed oxides at the initial scan and 100th scan respectively. Interestingly, the behavior of ternary oxide approaches similar to that of binary oxide after continuous cycling. The band structure in Fig. 5 indicates that the

equilibration of Fermi level is more compatible for Fe_2O_3 and SnO_2 and the potential at which the Fermi level is pinned in presence of alkali solution is nevertheless dominated by SnO_2. Therefore, there could be two plausible reasons that decrease the electrochemical capacitances of mixed oxides: (1) chemical or electrochemical passivation of either oxide; (2) Fermi level equilibration between the n- and p- type oxides that decides the stable state of charge. It is difficult to ascertain the exact reason, though either or both factors may play a role in deciding the electrochemical capacitance behavior of the ternary oxide.

4. CONCLUSIONS

We synthesized $CuO-SnO_2$ and $CuO-SnO_2-Fe_2O_3$ mixed oxides by hydrothermal method. In the search of new inorganic oxide materials for super capacitor applications, new combinations of mixed oxides such as $CuO-SnO_2$ and $CuO-SnO_2-Fe_2O_3$ were prepared by hydrothermal method and tried. Though the combination of SnO_2 with V_2O_5 (a semi-conductor) and Al_2O_3 (an insulator) gave very good results in our earlier works (Refs. 7 and 8), the same did not recur in the present work. CuO and Fe_2O_3 being transition metal oxides as well as insulating and semi-conducting oxides respectively, the electrochemical capacitances in combination with stannic oxide showed a negative effect. Unfortunately, they cannot be used as electrode materials for EDLC applications.

References

1. M. Jayalakshmi, K. Balasubramanian, *Int. J. Electrochem. Sci.,* 3 (2008) 1196.
2. F. Cao, J. Prakash, *J. Power Sources*, 92 (2001) 40.
3. Z. Fan, J. Chen, K. Cui, F. Sun, Y. Xu, Y. Kuang, *Electrochim Acta,* 52 (2007) 2959
4. A. R. de Souza, E. Arashiro, H. Golveia, T. A. F. Lassali, *Electrochim. Acta,* 49 (2003) 2015.
5. F. Pico, J. Ibañez, T. A. Centeno, C. Pecharroman, R. M. Rojas, J. M. Amarilla, J. M. Rojo, *Electrochim. Acta*, 51 (2006) 4693.
6. G. Bo, Z. Xiaogang, Y. Changzhou, L. Juan, Y. Long, *Electrochim. Acta,* 52 (2006) 1028.
7. M. Jayalakshmi, N. Venugopal, K. Phani Raja, M. Mohan Rao, *J. Power Sources,* 158 (2006) 1538.
8. M. Jayalakshmi, M. Mohan Rao, N. Venugopal, Kwang-Bum Kim, *J. Power Sources*, 166 (2007) 578.
9. N.-L. Wu, *Mater. Chem. Phys.* 75 (2002) 6.
10. A. A. F. Grupioni, E. Arashiro, T. A. F. Lassali, *Electrochim. Acta*, 48 (2002) 407.
11. J-K Chang, Y-L Chen, W-T Tsai, *J. Power Sources* 135 (2004) 344.
12. S. Bordoni, F. Castellani, F. Cavani, F. Trifiro, M. Gazzano, *J. Chem. Soc.Faraday Trans.* 90 (1994) 2981.
13. F. Scholz, U. Schröder, R. Gulaboski in: ̔Electrochemistry of immobilized Particles and Droplets ̓, Springer, Heidelberg, Germany, 2005.
14. M. Ming-you, H. Ze-qiang, X. Zhau-bing, H. Ke-long, X. Li-zhi, W. Zian-ming, *Trans. Nonferrous Met. Soc. China,* 16 (2006) 791.

15. M. Mohan Rao,_ M. Jayalaksmi, B. Ramachandra Reddy, S. S. Madhavendra, M. Lakshmi Kantam, *Chem. Lett.*, 34 (2005) 712.
16. M. Jayalakshmi, M. Mohan Rao, *J. Power Sources,* 157 (2006) 624.
17. K. Madhusudan Reddy, Babita Baruwati, M. Jayalakshmi, M. Mohan Rao, Sunkara V Manorama, *J. Solid State Chem.,* 178 (2005) 3352.
18. R.B. Vasiliev, M.N. Rumyantseva, S.E. Podguzova, A.S. Ryzhikov, L.I. Ryabova, A.M. Gaskov, *Mat. Sci. Eng*. B57 (1999) 241.
19. C.J. Fonstad, R.H. Rediker, *J. Appl. Phys.* 42 (1971) 2911.